Computers and Concrete, Vol. 9, No. 5 (2012) 341-355
DOI: http://dx.doi.org/10.12989/cac.2012.9.5.341

Compressive behavior of reinforced concrete columns confined by multi-spiral hoops

Y. Chen[1,2], J. Feng*[1,2] and S. Yin[3]

[1]*Key Laboratory of Concrete and Prestressed Concrete Structures of Ministry of Education, Southeast University, Nanjing, China*
[2]*National Prestress Engineering Research Center, Southeast University, Nanjing, China*
[3]*Ruentex Group, Shanghai, China*

(Received December 19, 2010, Revised July 9, 2011, Accepted August 11, 2011)

Abstract. Numerical studies are performed to predict the stress-strain behavior of rectangular RC columns confined by multi-spiral hoops under axial and eccentric compressions. Using the commercial finite element package ABAQUS, the Drucker-Prager criterion and the yield surface are adopted for damaged plasticity concrete. The proposed finite element models are compared with the published experimental data. Parametric studies on concrete grades, confinement arrangement, diameter and spacing of hoops and eccentricity of load are followed. Numerical results have shown good agreements with experimental values, and indicated a proper constitutive law and model for concrete. Cross-sectional areas and spacing of the hoops have significant effect on the bearing capacity. It can be concluded that rectangular RC columns confined by multi-spiral hoops show better performance than the conventional ones.

Keywords: multi-spiral hoops; damaged plasticity concrete; confinement; axial compression; eccentricity.

1. Introduction

The strength and ductility of a concrete member can be significantly increased by confining transverse reinforcements, thus the relevant investigation has become increasingly popular currently. Because spiral hoops have better confining effectiveness than general rectangular stirrups, they have been widely used in circular and elliptical concrete members. The study of applying spiral hoops in concrete columns will become increasingly important, especially in Asia, due to the large proportion of RC structures.

With the development of computers and finite element simulation techniques, it has become a cost-effective way to study RC structures using finite element methods (FEM) together with a relative small number of experiments. Karabinis *et al.* (2008) carried out a numerical study on RC columns confined by FRP wrap. Eid *et al.* (2006) used a 2D FEM to study the linear elastic confinement behavior and showed that tie spacing and cross sectional areas affect the capacity of circular columns. Rapid development of finite element technologies promotes numerical simulations becoming easier. But the nonlinear compressive behavior of concrete is still a hard work, because of the cracks and their influence on the damage of structural stiffness. Kwon and Spacone (2002) investigated the effect of confinement mechanism on the concrete cylinders using a smeared crack approach, to reasonably explain the significant phenomena observed from the tests. Papanikolaou

* Corresponding author, Professor, E-mail: fengjian@seu.edu.cn

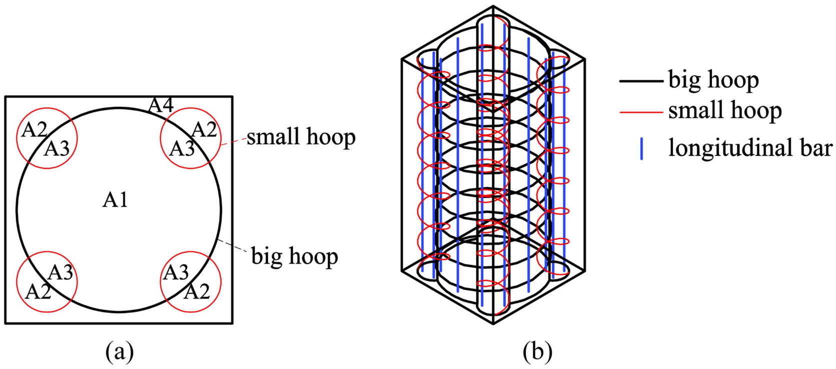

Fig. 1 A typical rectangular RC column confined by multi-hoops: (a) plan view, (b) in 3D

and Kappos (2009) presented a finite element analysis on the confinement effects for concrete bridge piers with a detailed parametric study for concrete with various concrete strengths, reinforcement arrangements and tie spacing. It has demonstrated that 3D nonlinear finite element analysis is able to investigate the confinement effects in RC columns, especially for those with complicated geometry. Campione and Fossetti (2007) investigated the compressive behavior of a short concrete elliptical column confined by single spiral hoop with FEM, using the compressive stress-strain relationship by Mander *et al*. (1988). It demonstrated a good accordance with experimental results. However, the studies on rectangular RC columns confined by spiral hoops are limited. Majewski *et al.* (2008) investigated the failure behavior of rectangular columns under eccentric loads. But, it shall be stated that assuming plane strain condition for 3D concrete properties results into a slightly higher capacity than the experimental values.

In order to fully utilize the confining effect of spiral hoops for rectangular RC columns, Yin (2008) proposed a confining type with multi-hoops by using a big hoop for the centre region and four small hoops at the corners, as shown in Fig. 1: A_1 and A_2 denote the areas of the concrete confined by the big and the small hoops respectively, A_3 is the area of the concrete confined by both and A_4 is the unconfined area.

The small hoops are welded to the longitudinal bars in angles, so that they can provide additional support to the longitudinal bars to prevent premature buckling. This innovative confinement type has been validated by series of experiments (Yin 2008, Weng *et al*. 2008, Chiang 2009), and has started to be adopted in practical use by precast construction industry. The study here adopts FEM with damaged plasticity model to investigate the novel behaviors of columns confined by multi-hoops, and seeks to provide some information suitable for predicting the compressive behavior of rectangular RC columns under monotonic axial and eccentric loads.

2. Method

2.1 Modified concrete constitutive law by Mander

A reasonable constitutive concrete law is very important for predictions on concrete columns. Various constitutive laws for confined concrete have been proposed in recent years. Mander *et al.*

(1988) proposed a constitutive law especially for concrete in RC columns, as in Eqs. (1-4). It is a semi-empirical expression obtained from tests for RC columns with various cross-sections and reinforcement arrangements, and it has been widely adopted for confined concrete research by different investigators ever since.

$$f_c = \frac{f'_{cc}E_c\varepsilon_c/\varepsilon_{cc}}{E_{\sec}+(E_c-E_{\sec})(\varepsilon_c/\varepsilon_{cc})^{E_c/(E_c-E_{\sec})}} \tag{1}$$

where f_c is the compressive concrete stress, $E_c = 5000\sqrt{f'_{c0}}\ MPa$ is the tangent modulus of elasticity, $E_{sec} = f'_{cc}/\varepsilon_{cc}$ is the secant modulus.
f'_{cc} and ε_{cc} are the maximum compressive stress and strain correspondingly, given as

$$f'_{cc} = f'_{c0}(-1.254+2.254\sqrt{1+7.94f'_l/f'_{c0}}-2f'_l/f'_{c0}) \tag{2}$$

$$\varepsilon_{cc} = \varepsilon'_{c0}(1+5(f'_{cc}/f'_{c0}-1)) \tag{3}$$

where the strain ε'_{c0} is taken as 0.002, and it corresponds to nominal compressive strength (f'_{c0}) of plain concrete with a standard prism geometry.

The effective lateral confining stress on the concrete f'_l is

$$f'_l = \frac{\pi d^2(1-0.5(s-d)/D)}{DS(2-2A_s/A_c)}f_y \tag{4}$$

where A_c is the area of the confined core concrete, A_s is the area of longitudinal bars, f_y is the yield strength of hoops, s is the spacing of the spirals, D is the diameter of the spirals, and d is the diameter of the spiral rebar. An illustrative stress-strain relationship for confined concrete (Eqs. (1-4)) is shown by the top thin curve in Fig. 2.

By taking $f'_l = 0$, $f'_{cc} = f'_{co}$, Eqs. (1-4) give the stress-strain relationship for unconfined plain concrete, as shown by the lowest dot-dash curve in Fig. 2: this relationship is modified to give a strain-softening curve when $\varepsilon_c > 2\varepsilon'_{c0}$, and the maximum compressive strain is taken as the spalling strain ε_{sp}=0.005. Under tension, concrete behaves linearly elastically to the tensile strength f'_{t0}, before softening following a curved strain-softening relationship, shown by the left thick curve in Fig. 2.

Known from Eqs. (1-4), the compressive stress for a piece of confined concrete depends on f_{c0}, f_c and f'_l, and thus can be expressed by a function $f_c = F_1(\varepsilon_c, f'_{c0}, f_y, A_c, A_s, s, D, d)$; whilst the

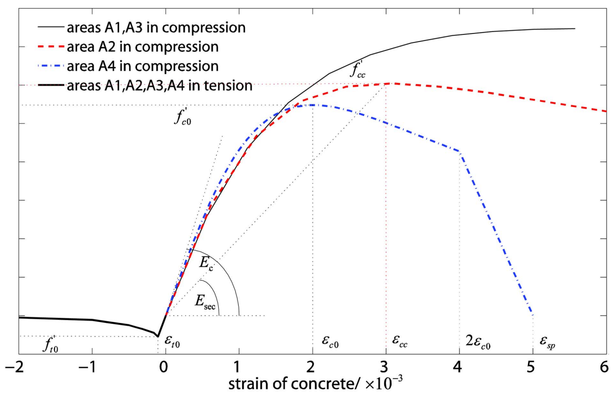

Fig. 2 Concrete constitutive relations of Column M1

compressive stress for unconfined concrete depends only on f'_{c0}, and therefore $f_c = F_2(\varepsilon_c, f'_{c0})$.

Hence, the concrete compressive stress-strain relationship for different locations, areas A_1, A_2, A_3 and A_4 (shown in Fig. 1), are as follows

$$f_{ci} = F_1(\varepsilon_{ci}, f'_{c0}, f_{yi}, A_{ci}, A_{si}, s_i, D_i, d_i), \quad i = 1,2 \tag{5}$$

$$f_{c3} = \max(f_{c1}, f_{c2}) \tag{6}$$

$$f_{c4} = F_2(\varepsilon_{c4}, f'_{c0}) \tag{7}$$

Concrete constitutive law proposed by Hognestad (1955) is also considered, and compared with that of Mander *et al.* (1988). The compressive stress-strain curve of Hognestad is a parabolic curve where $\varepsilon_c \le \varepsilon'_{c0}$, and a downward straight line where $\varepsilon'_{c0} < \varepsilon_c \le \varepsilon_{sp}$, expressed as

$$f_c = \begin{cases} f'_{c0}\left(\dfrac{2\varepsilon_c}{\varepsilon'_{c0}} - \left(\dfrac{\varepsilon_c}{\varepsilon'_{c0}}\right)^2\right) & 0 \le \varepsilon_c \le \varepsilon'_{c0} \\ f'_{c0}\left(1 - 0.15\dfrac{\varepsilon_c - \varepsilon'_{c0}}{\varepsilon_{sp} - \varepsilon_0}\right) & \varepsilon'_{c0} < \varepsilon_c \le \varepsilon_{sp} \end{cases} \tag{8}$$

where $\varepsilon'_{c0} = 0.002$ and $\varepsilon_{sp} = 0.0038$.

2.2 Damaged plasticity model for concrete

Abu-Lebdeh and Voyiadjis (1993) adopted plasticity and damage mechanics to assess the monotonic behavior of concrete. They found that the hardening behavior of concrete could be described by damage and plasticity. Grassl *et al.* (2002) carried out a theoretical study on compressive behavior of plain concrete under uniaxial, biaxial and triaxial conditions based on plasticity theory and presented good agreements with experimental results. The distinctive degradation of the mechanical properties of concrete under compressions has been well predicted by plasticity-damage theory (Voyiadjis *et al.* 2008). Fortunately, in the material library of ABAQUS (ABAQUS Version 6.6 2005), there has been a novel damaged plasticity concrete model suitable for representing the irreversible damage of structural stiffness. The stress-strain relation of the damaged plasticity concrete could be expressed as

$$\varepsilon = \sigma/((1-\chi)E_0) + \varepsilon_p \tag{9}$$

where ε and ε_p are the strain and plastic strain of concrete, σ is the stress of concrete; χ is the damage variable, ranging from zero (undamaged state) to one (fully damaged state), and E_0 is the corresponding elastic stiffness of the undamaged concrete. In this model, concrete damage is classified by using flow potential and yield surface given as follows

Drucker-Prager function gives

$$G = \sqrt{(\in \sigma_{t0} \tan\psi)^2 - \bar{q}^2} - \bar{p}\tan\psi \tag{10}$$

where $\in$ is the flow potential eccentricity (taken as 0.1), σ_{t0} is the uniaxial tensile stress at failure, ψ is the dilation angle (taken as 30°), $\bar{q}$ is the von Mises equivalent effective stress and $\bar{p}$ is the hydrostatic pressure stress.

A yield criterion modified by Lee *et al* (1998) from Lubliner *et al* (1989) is adopted as

$$Y = \frac{1}{1-\alpha}(\bar{q} - 3\alpha\bar{p} + \beta\bar{\sigma}_{\max} - \gamma(-\bar{\sigma}_{\max})) = 0$$

$$\alpha = \frac{\sigma_{b0}/\sigma_{c0} - 1}{2\sigma_{b0}/\sigma_{c0} - 1},\ \beta = \frac{\bar{\sigma}_c}{\bar{\sigma}_t}(1-\alpha) - (1+\alpha),\ \gamma = \frac{3-3K_c}{2K_c - 1} \tag{11}$$

where $\bar{\sigma}_{\max}$ is the maximum principal effective stress; σ_{b0}/σ_{c0} is the ratio of the initial equi-biaxial compressive yield stress to the initial uniaxial compressive yield stress (taken as 1.17); $\bar{\sigma}_c$ and $\bar{\sigma}_t$ are the effective compressive and tensile cohesion stress respectively; K_c is the ratio of the second invariant of stress tensor on the tensile meridian to that on the compressive meridian, and it is treated as a constant parameter for concrete as 0.667.

2.3 Finite element modelling

The commercial finite element package ABAQUS is used to predict the compressive and tensile behavior of rectangular RC columns confined by multi-spiral hoops. The concrete in the columns are modeled by 8-node linear brick element, with reduced integration and hourglass control. These elements are isotropic in tension and follow the above plastic damage rules under compression. Most concrete are meshed using a character size of 30 mm, where the mesh is doubly refined near the cylinder surfaces, to obtain an accurate solution and a satisfied stress distribution near the spiral hoops, shown in Figs. 3(a-b). The steel reinforcements are meshed by 3-node quadratic displacement

Table 1 Mechanical properties adopted for the models

Material	Parameters			
	Elastic modulus E (GPa)	Poisson's ratio μ	Specific gravity (T/m^3)	Inelastic behavior
Reinforcement	206	0.3	7.85	Elastic-perfect plastic
concrete	26.17	0.2	2.4	refer to Eqs. (5-7)

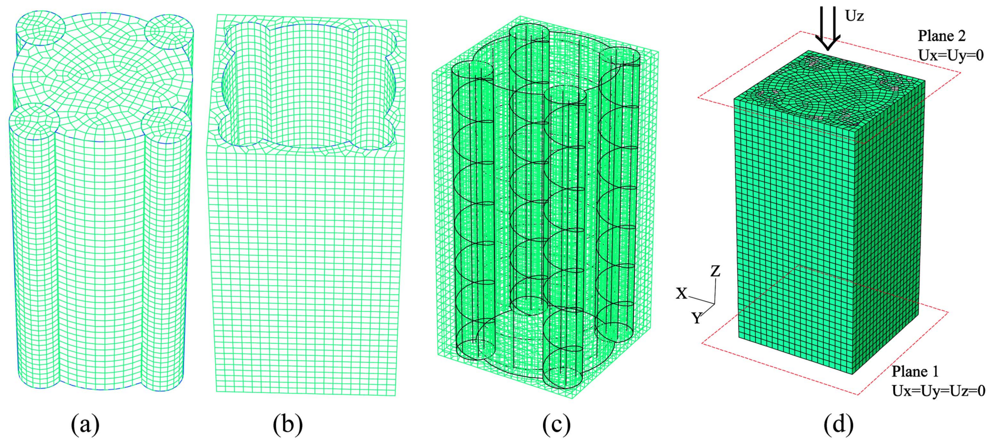

Fig. 3 Concrete and reinforcement modelling and boundary conditions: (a) finite element mesh for confined concrete, (b) mesh for cover concrete, (c) embedded hoops and bars, (d) boundary conditions and the prescribed displacement

truss elements, embedded in concrete elements (Fig. 3(c)), and with the von Mises elastic-perfect plastic behavior. The detailed parameters for describing the behaviors of concrete and steel elements are shown in Table 1.

Moreover, to avoid concentrations of stress and to guarantee the boundary conditions in accord with experiments, automatic node-to-surface contacts are applied between the column and the two rigid planes, as illustrated in Fig. 3(d). The prescribed displacement boundary conditions are applied on the top rigid plane to compress the RC columns.

To improve the convergent rate without compromising results, the viscosity parameter is set as 10^{-5} for the plastic damage criterion. In addition, geometric nonlinearity is activated to consider the second effect of eccentric load and lateral displacement when columns are in eccentric compressions, though the effect is limited due to the small length to width ratio.

3. Results and discussions

3.1 Validation of the confined concrete stress-strain relation

Kupfer *et al*. (1969) gave stress-strain curves of plain concrete based on a number of uniaxial and

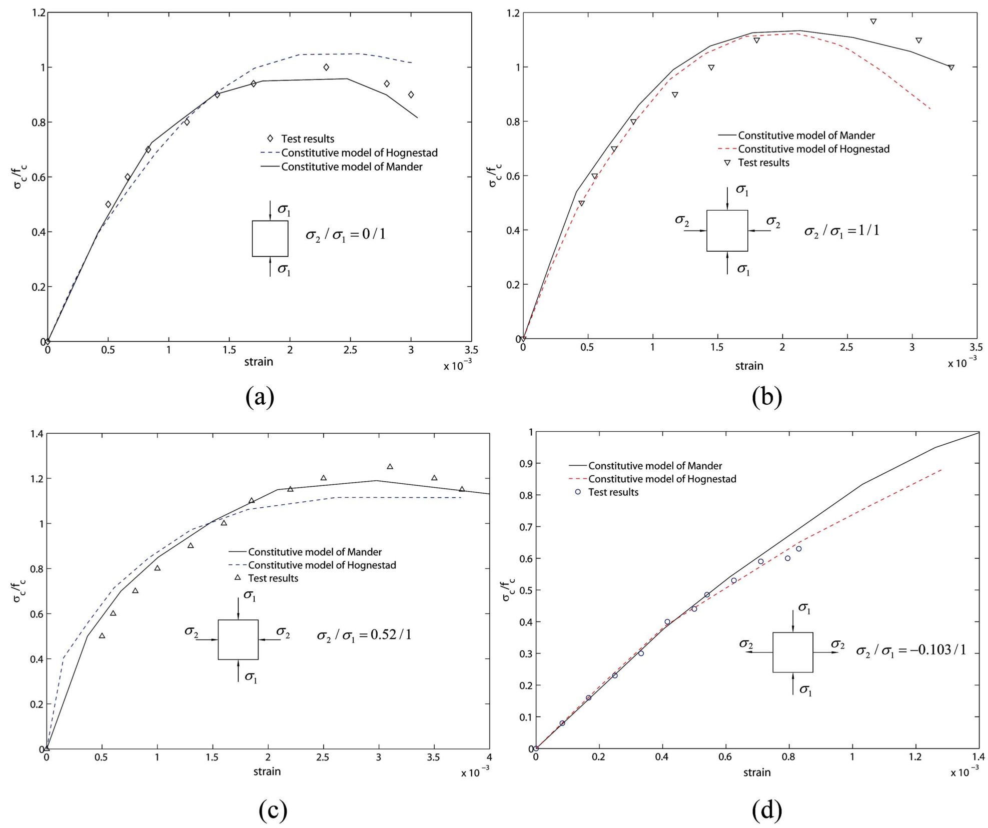

Fig. 4 Stress-strain relations under: (a) uniaxial compression, (b-c) biaxial compressions, (d) tension and compression

biaxial compression experiments, and applied these result to aid simulating the compressive behavior of confined concrete. These data are used to validate the constitutive relations and the plastic damaged model aforementioned. The results are as shown in Fig. 4, where σ/f_c is used as a normalized stress measurement.

Both the numerical results got by Mander's $\sigma-\varepsilon$ curve and those using Hognestad's one agree well with the experimental results from Kupfer. But, the discrepancies of the former are smaller. Therefore, the constitutive relation proposed by Mander is adopted here. Also, as illustrated in Figs. 4(b-c), the normalized stress of plain concrete under biaxial compressions is higher than that under uniaxial compression, and with a quantitative ratio of around σ_{b0}/σ_{c0} = 1.17 (refer to Eq. (11)), which confirms its value adopted for damaged plasticity concrete use.

3.2 Numerical results

Fig. 5 shows different confinement types M, N, and G, which are used to confine rectangular columns.

A total of 9 columns with type M (M1-M3), type N (N1-N3) and type G (G1-G3) have been studied as the referenced columns. Table 2 lists their configurations, and gives their bearing capacities obtained from Test and FEM.

Both type M and type N belong to the multi-spiral hoops confinement type, where type N is from

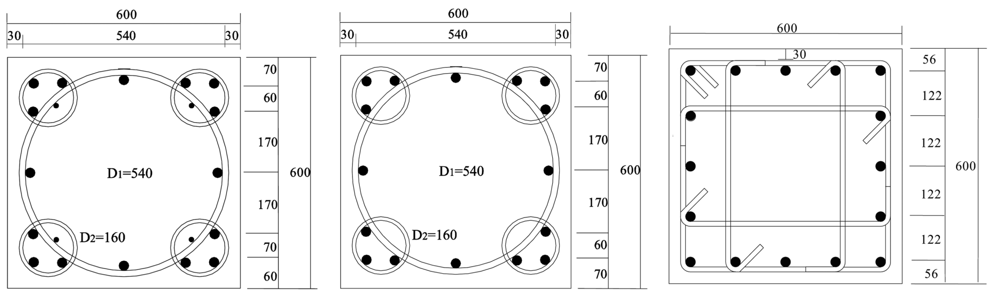

Fig. 5 Different confinement type patterns: (a) Type M, (b) Type N, (c) Type G

Table 2 Configurations and numerical results of columns M1-M3, N1-N3 and G1-G3

Column	s_1 /mm	s_2 /mm	d_1 /mm	d_2 /mm	f'_{c0} /MPa	Longitudinal bar types	Eccentricity *e*/mm	Bearing capacity/kN		
								Test	FEM	Error/%
M1	146	189	16	10	27.4	16**d*25+4**d*13	0	16200	16823	3.846
N1	146	189	16	10	27.4	16**d*25	0	/	16600	/
G1	123		13		27.4	16**d*25	0	13500	12550	7.037
M2	117	151	16	10	34.3	16**d*25+4**d*13	0	19083	20230	6.011
N2	117	151	16	10	34.3	16**d*25	0	/	20007	/
G2	123		13		34.3	16**d*25	0	16920	15221	10.041
M3	54	189	10	6	50	16**d*25+4**d*16	400	4082	4101	0.465
N3	54	189	10	6	50	16**d*25	400	3964	3858	2.674
G3	50		10		50	16**d*25	400	3810	3710	2.625

type M by removing the four longitudinal slender bars. Type G is a general confinement type, where columns confined by rectangular stirrups (G1-G3) have an identical volume ratio of stirrups, ρ_s, to those confined by type M (M1-M3). Columns M1/N1/G1-M2/N2/G2 which have a column length of 1200 mm and a spiral diameter D_2 of 160 mm are under axial compressions, while rest columns with a column length of 2000 mm and a spiral diameter D_2 of 150 mm subject to eccentric loads. Sizes of cross section for all the columns are 600 mm × 600 mm, the yield stresses of the reinforcements $f_y = 412$ MPa, the central spiral diameter $D_1 = 540$ mm, and the thickness of cover concrete $c = 30$ mm.

Numerical results of complete compressive behavior of RC columns are compared with available experimental data from tests on physical models (Yin 2008, Chiang 2009). They are discussed in terms of axial and eccentric compressions, respectively.

3.2.1 Axial compression

The stress-strain curves of columns under axial compression are shown in Fig. 6, with different confinement types and concrete grades considered. It should be noted that the axial strains shown in Fig. 6 are defined as the axial displacements divided by heights of the column, and the axial stresses are defined as the bearing load of concrete plus bars divided by gross section area.

It can be observed from Fig. 6 that the numerical results obtained by ABAQUS agree well with the discrete experimental values. The maximum relative error of columns confined by multi-spiral hoops (types M and N) is 6.01%, while that of columns with general confinement type G is 10.04%. From the comparisons between types M1-M2 and types N1-N2, the axial stress of type N columns are appreciably lower than those of type M. Thus, the four removed longitudinal bars show a slight effect on the bearing capacity and ductility. Compared to results of columns which are confined by general stirrups and have the same volume ratio of stirrups, the bearing capacity and ductility of columns confined by multi-spiral hoops are raised by 33% and 145%, respectively. Moreover, the column with a lower concrete grade is proved to have a better enhancement.

Numerical simulations of different parts of a typical column with type M1 are exhibited in Fig. 7 at the limit step, where the external load just reaches the limit condition of the bearing capacity.

Although the information about distributions of stress and strain, and crack patterns is hard to measure in a test specimen, they could be easily generated by FEM. As shown in Fig. 7(a), the

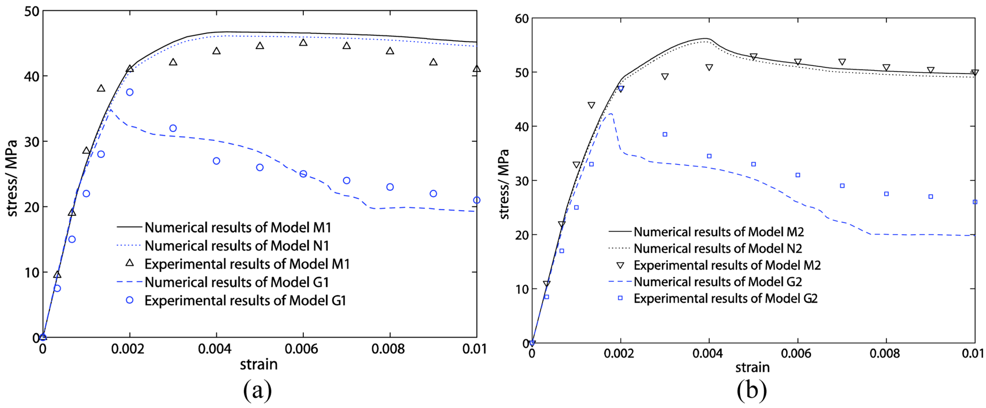

Fig. 6 Stress-strain curves: (a) type M1, N1 and G1, (b) type M2, N2 and G2

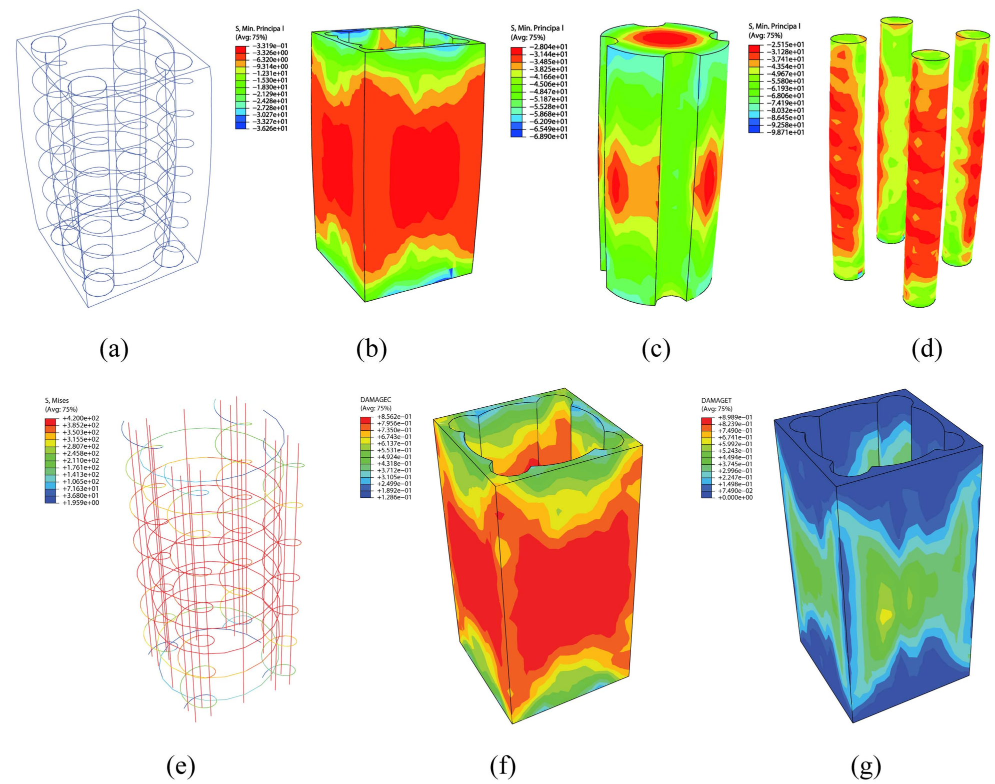

Fig. 7 Numerical results: (a) deformed shape (scale: 1:20), (b-d) principal stress contour of areas A_4, A_1 and areas A_2 and A_3, respectively, (e) stress contour of steel elements, (f-g) compressive and tensile damage contour of area A_4

column gradually deforms in a mode of outward expansion with the increase of the axial load. Figs. 7(f-d) show the damage contour of the cover concrete, where the damage criterion could refer to Eqs. (9-11). It can be found from Figs. 7(b), (f) and (g) that, most of the cover concrete has been spalled off completely when the load reaches the ultimate bearing capacity. Fig. 7(e) illustrates that all the steel spiral hoops and bars have been into the yield condition. Because the main and the other small spiral hoops are continuous and interacting with each other, concrete located in areas of $A1$, $A2$ and $A3$ are well confined (Figs. 7(c-d)). That is one reason why this new confinement type is very popular in the rectangular RC columns.

3.2.2 Eccentric compression

Eccentric load-lateral displacement curves for both the numerical and experimental results of columns with type M3, N3 and G3 are shown in Fig. 8, respectively.

As the boundary conditions for the column models under eccentric compressions are not perfectly equivalent with the setups in the experiments, there is a slight difference between the initial rigidity of the numerical models and the physical columns. Consequently, the numerical results are larger than the experimental ones before occurrences of the first crack. Then numerical results agree well with the discrete experimental values, where the maximum relative error is 2.67%. The curves of columns M3 and N3 demonstrate that, the ultimate eccentric bearing load of column M3 is 1.03

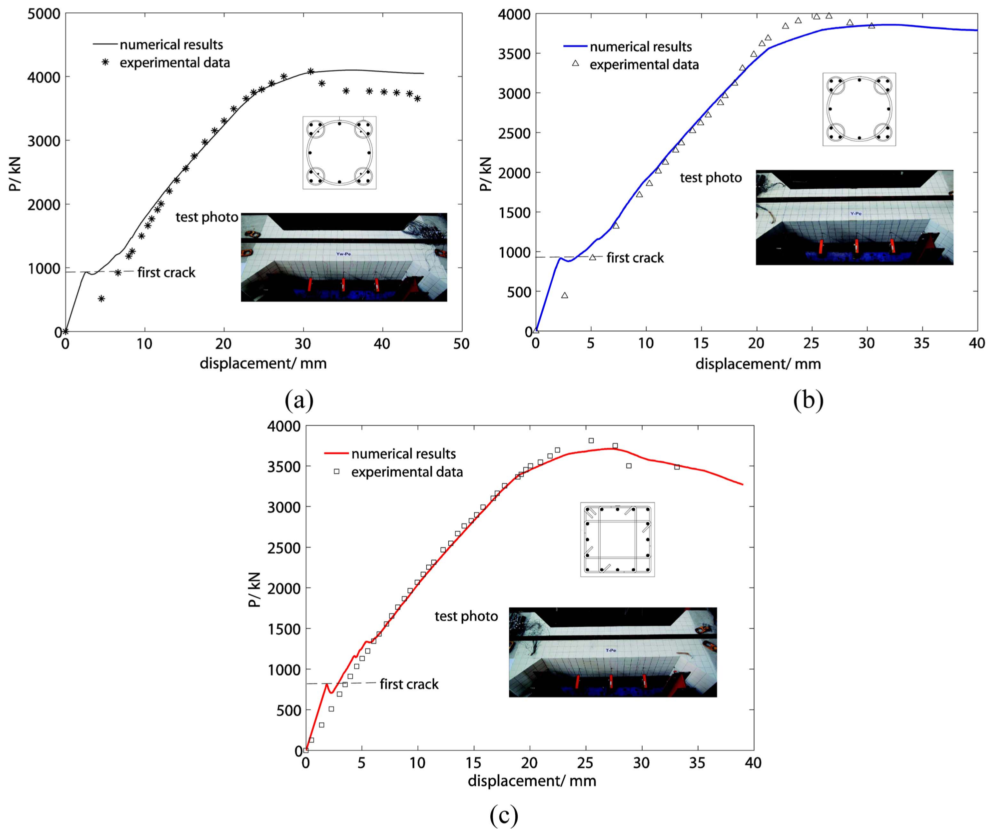

Fig. 8 Load-displacement curves: (a) type M3, (b) type N3, (c) type G3

times that of column N3, while the corresponding lateral displacement of column M3 is 1.16 times that of column N3. Thus, removing the four thin bars has a slight negative effect on the bearing capacity and ductility of the column. Compared the ultimate eccentric bearing load of columns M3 with the result of column G3, it explains the bearing capacity and ductility of a column will be enhanced by 7.14% and 21.4%, if the general confinements are substituted by multi-spiral hoops, with volume ratio of stirrups and other parameters kept identical.

With the first cracks appearing in the columns, the stiffness loss and drops of stress in some concrete elements happen. Thus, severe drop appears at the beginning of each load-displacement curve of the columns M3, N3 and G3. Then the cracks will keep developing, and the damage variables will increase accordingly. Concerned the ultimate condition, numerical simulations of the multi-spiral hoops column M3 under eccentric compression are shown in Fig. 9.

As shown in Fig. 9(a), the column gradually deforms towards the lateral direction paralleled to the direction of eccentricity, where the eccentricity is enlarged by the increasing load. Because the column is under eccentric compression, the stresses of concrete and spiral hoops which are close to the axis of the eccentric load are much higher than that far from the axis. Consequently, the small spiral hoops lay in the far side (Fig. 9(c)) have negligible confinement effectiveness. The severe damages existed along half height of the column (Fig. 9(d)) reveal those vertical cracks which have been observed from experiments (shown in Fig. 9(e)).

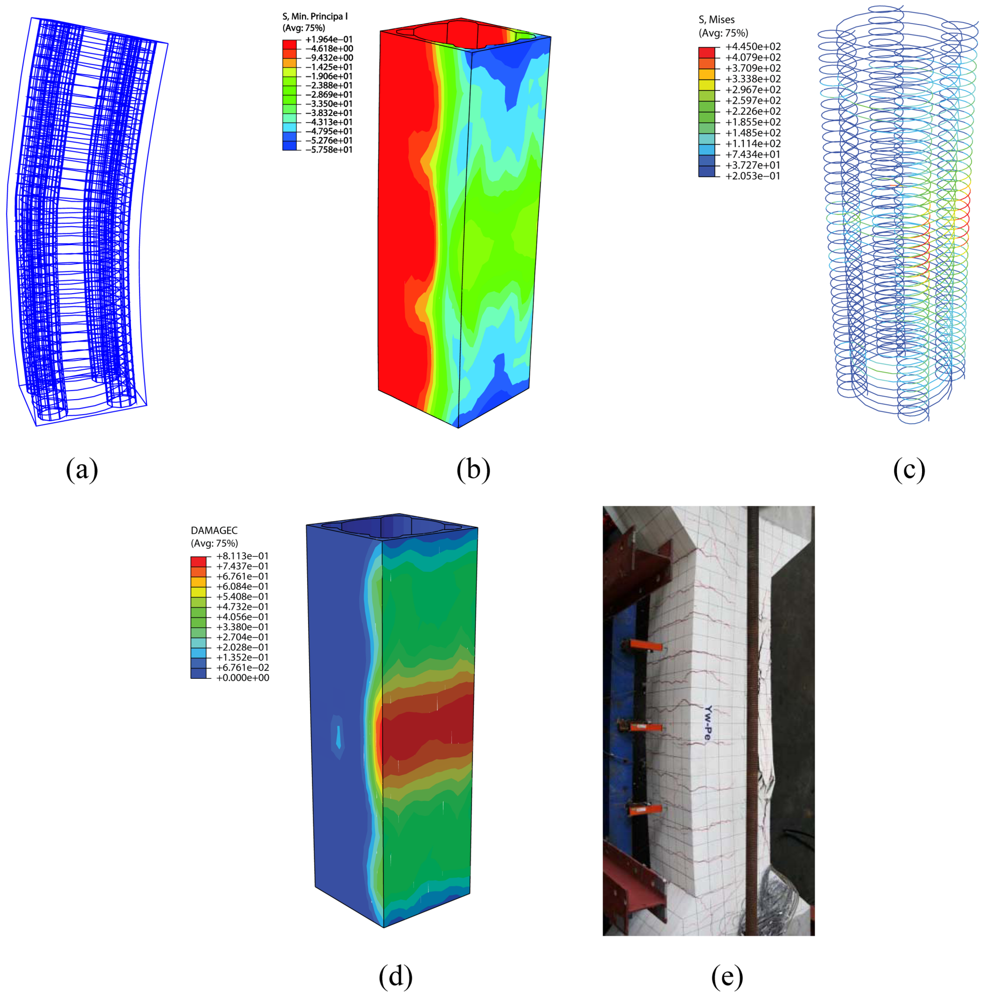

Fig. 9 Numerical results of column M3: (a) deformed shape (scale: 1:10), (b) principal stress contour graph of area A_4, (c) stress contour of multi-spiral hoops, (d-e) compressive damage graph and the actual column model at failure

3.3. Parametric studies

3.3.1. Studies for columns under axial compression

The effects of confinement arrangements and concrete grades have been investigated in section 3.1. In this section, suitable parametric studies are arranged to examine the parameters included spacing, diameters of big and small spiral hoops and cross-sectional areas of the hoops. The full column is listed in compact form (Table 3) for easy reference, with column M1 considered as the referenced model.

Fig. 10 shows a typical histogram for the complete range of columns confined by type M.

From the interpretation of all available numerical values for the columns, cross-sectional areas have the most significant effect on the bearing capacity. Ultimate strength of column M12 and M13 are raised by 5.45% and 13.0%, with the ductility raised by 18.4% and 47.2% respectively, due to

Table 3 RC columns M4-M13 under axial compressions (1 indicates 'yes')

Column	s_1/mm			D_1/mm			D_2/mm			d_1/mm			d_2/mm		
	106	126	146	500	520	540	140	150	160	10	13	16	10	13	16
M1			1			1			1			1	1		
M4		1				1			1			1	1		
M5	1					1			1			1	1		
M6			1	1					1			1	1		
M7			1		1				1			1	1		
M8			1			1	1					1	1		
M9			1			1		1				1	1		
M10			1			1			1	1			1		
M11			1			1			1		1		1		
M12			1			1			1			1		1	
M13			1			1			1			1			1

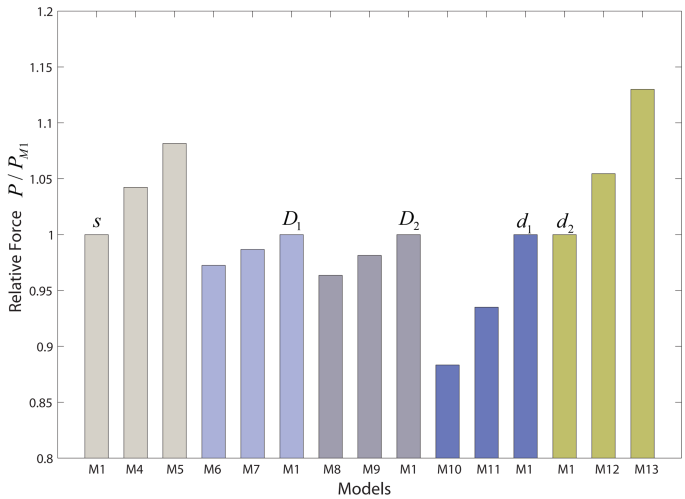

Fig. 10 Typical histogram for the complete range

the increase of the hoop diameter, d_2. Meanwhile, the ultimate strength is also sensitive to the spacing of hoops. It increases about 4.16% with a spacing decrease of 20 mm. Thus, it could be stated that smaller transverse reinforcement spacing contributes more to confinement effectiveness.

Although the confined areas are enlarged by the increase of the spiral diameter, D_1 or D_2, the effective lateral confining stress denoted in Eq. (4) is reduced. Therefore, pure increase of the spiral diameter has a poor efficiency of the confinement. According to the definition of relative volumetric mechanical ratio of spiral reinforcement among core and corner regions, the volume ratio of spiral hoops, ρ_s, could be written as

$$\rho_s = \frac{\pi D_1 A_{sp1} + 4\pi D_2 A_{sp2}}{s A_C} \tag{12}$$

where $A_{sp1} = \frac{\pi d_1^2}{4}$, $A_{sp2} = \frac{\pi d_2^2}{4}$ are the cross section areas of big and small hoops, and A_C is the gross section area of column. Based on the different parameters in Table 3 and the corresponding results (see Fig. 10), it could be concluded that the optimum relative volumetric mechanical ratio is $\rho_s = 1.43\%$.

3.3.2 Effect of eccentricity e

Columns G4-G13 and M14-M23 are also studied to consider the effect of the eccentricity $\bar{e}$ under eccentric compressions, listed in Table 4. The dimensionless eccentricity is denoted as $\bar{e} = e/B$, where B is the bottom length of the rectangular cross section ($B = 600$ mm in this study). Except for the eccentricity, e, all the other configurations of columns G4-G13 and M14-M23 are identical to column G3 and M3, respectively.

The relation curves between the ultimate reaction moments and the ultimate reaction forces are shown in Fig. 11.

The curves reveal that columns of type M have better performance than columns of type G, in terms of resisting the eccentric loads. Both the ultimate reaction forces reach their maximum when columns are under axial loads, that is $\bar{e} = 0$. The ultimate forces of both types of columns are reduced by the increase of the moments for $\bar{e} \leq 0.333$. On the contrary, they are raised by the moments when $\bar{e} > 0.333$. For columns of type G and type M, averagely 19.1% of the ultimate reaction forces are reduced by every increase of $\bar{e} = 0.083$ for the dimensionless eccentricity.

Table 4 RC columns G4-G13 and M14-M23 under eccentric compressions

Columns												
Columns	Type G	G3	G4	G5	G6	G7	G8	G9	G10	G11	G12	G13
	Type M	M3	M14	M15	M16	M17	M18	M19	M20	M21	M22	M23
Dimensionless *e*		0.667	0	0.083	0.167	0.25	0.333	0.417	0.5	0.583	0.75	0.833

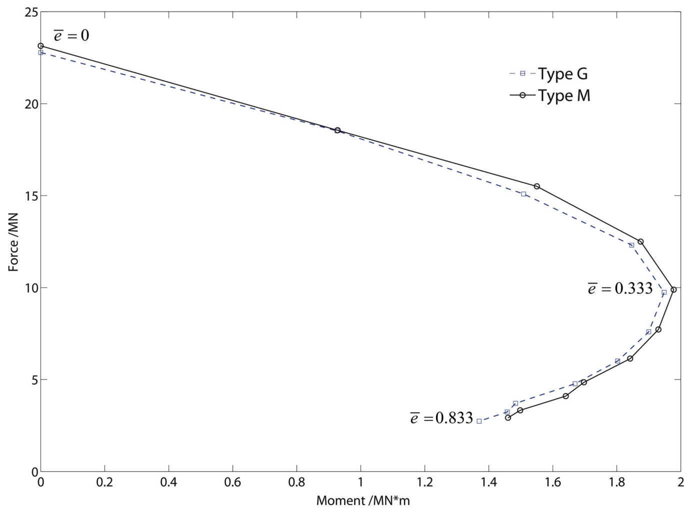

Fig. 11 Moment-Force curves of different confinement types

4. Conclusions

In this paper, the compressive behavior of rectangular RC columns has been studied. Numerical results show good agreements in terms of general compressive behavior with the experimental data under axial and eccentric compressions. It can be concluded that: The new multi-spiral hoops confinement type is effective to restrict the transverse displacements of rectangular concrete columns. The strength and ductility of columns confined by multi-spiral hoops are raised by 33% and 145% under axial compression respectively, and are raised by 7.14% and 21.4% under eccentric compression with a dimensionless eccentricity of $\bar{e} = 0.667$ correspondingly. Cross-sectional area of hoops affects the bearing capacity of columns subjected to axial loads significantly: the strength and ductility would be raised by 2.56% and 11.25%, if the cross-sectional area of spiral hoops rises by 10%. In addition, each increase of 0.083 for the dimensionless eccentricity will reduce about 0.191 times of the ultimate reaction forces.

Acknowledgments

This work was supported by the Priority Academic Program Development of Jiangsu Higher Education Institutions of China, and Scientific Research Foundation of Graduate School of Southeast University (Grant No. YBJJ1025). Special thanks go to Mr. Garfield Guan from Advanced Structures Group at the University of Cambridge, and Dr. Yixiang Xu from Department of Civil Engineering at Strathclyde University for their valuable comments throughout this work. Suggestions from the reviewers are also gratefully acknowledged.

References

ABAQUS Version 6.6 on-line documentation (2005), *ABAQUS analysis user's manual*, Abaqus Inc.

Abu-Lebdeh, T.M. and Voyiadjis, G.Z. (1993), "Plasticity-damage model for concrete under cyclic multiaxial loading", *J. Eng. Mech.-ASCE*, **119**(7), 1465-1484.

Campione, G. and Fossetti, M. (2007), "Compressive behavior of concrete elliptical columns confined by single hoops", *Eng. Struct.*, **29**(3), 408-417.

Chiang, P.C. (2009), *Mechanical analysis of 5-spiral stirrup concrete column*, Thesis of Taiwan University, Taipei. (in Chinese)

Eid, R. and Dancygier, A.N. (2006), "Confinement effectiveness in circular concrete columns", *Eng. Struct.*, **28**(13), 1885-1896.

Grassl, P., Lundgren, K. and Gylltoft, K. (2002), "Concrete in compression: a plasticity theory with a novel hardening law", *Int. J. Solids. Struct.*, **39**(20), 5205-5223.

Hognestad, E. (1955), "Concrete stress distribution in ultimate strength design", *J. ACI*, **52**(12), 455-480.

Karabinis, A.I., Rousakis, T.C. and Manolitsi, G.E. (2008), "3D finite-element analysis of substandard RC columns strengthened by fiber-reinforced polymer sheets", *J. Compos. Constr.*, **12**(5), 531-540.

Kupfer, H., Hilsdorf, H.K. and Rusch, H. (1969), "Behavior of concrete under biaxial stresses", *J. ACI*, **66**(52), 656-666.

Kwon, M. and Spacone, E. (2002), "Three-dimensional finite element analyses of reinforced concrete columns", *Comput. Struct.*, **80**(2), 199-212.

Lee, J. and Fenves, G. (1998), "Plastic-damage model for cyclic loading of concrete structures", *J. Eng. Mech.*, **124**(8), 892-900.

Lubliner, J., Oliver, J., Oller, S. and Onate, E. (1989), "A plastic-damage model for concrete", *Int. J. Solids.*

Struct., **25**(3), 299-329.
Majewski, T. Bobinski, J. and Tejchman, J. (2008), "FE analysis of failure behavior of reinforced concrete columns under eccentric compression", *Eng. Struct.*, **30**(2), 300-317.
Mander, J.B. Priestly, M. and Park, R. (1988), "Theoretical stress-strain model for confined concrete", *J. Struct. Eng.-ASCE*, **114**(8), 1804-1826.
Papanikolaou, V.K. and Kappos, A.J. (2009), "Numerical study of confinement effectiveness in solid and hollow reinforced concrete bridge piers: Analysis results and discussion", *Comput. Struct.*, **87**(21-22), 1440-1450.
Papanikolaou, V.K. and Kappos, A.J. (2009), "Numerical study of confinement effectiveness in solid and hollow reinforced concrete bridge piers: Methodology", *Comput. Struct.*, **87**(21-22), 1427-1439.
Voyiadjis, G.Z., Taqieddina, Z.N. and Kattan, P.I. (2008), "Anisotropic damage-plasticity model for concrete", *Int. J. Plasticity*, **24**(10), 1946-1965.
Weng, C.C., Yin, S., Wang, J.C. and Liang, C.Y. (2008), "Seismic cyclic loading test of SRC columns confined with 5-Spirals", *Sci. China Ser. E.*, **51**(5), 529-555.
Yin, S. (2008), "Design and construction innovations for reinforced concrete structures", *The 3rd ACF international conference ACF/VCA*, Ho Chi Minh city, Vietnam.

CC